Stu2p binds tubulin and undergoes an open-to-closed conformational change

Jawdat Al-Bassam,[1] Mark van Breugel,[3] Stephen C. Harrison,[1,2] and Anthony Hyman[3]

[1]Department of Biological Chemistry and Molecular Pharmacology and [2]Howard Hughes Medical Institute, Harvard Medical School, Boston, MA 02115
[3]Max Planck Institute of Molecular Cell Biology and Genetics, 01307 Dresden, Germany

Stu2p from budding yeast belongs to the conserved Dis1/XMAP215 family of microtubule-associated proteins (MAPs). The common feature of proteins in this family is the presence of HEAT repeat–containing TOG domains near the NH_2 terminus. We have investigated the functions of the two TOG domains of Stu2p in vivo and in vitro. Our data suggest that Stu2p regulates microtubule dynamics through two separate activities. First, Stu2p binds to a single free tubulin heterodimer through its first TOG domain. A large conformational transition in homodimeric Stu2p from an open structure to a closed one accompanies the capture of a single free tubulin heterodimer. Second, Stu2p has the capacity to associate directly with microtubule ends, at least in part, through its second TOG domain. These two properties lead to the stabilization of microtubules in vivo, perhaps by the loading of tubulin dimers at microtubule ends. We suggest that this mechanism of microtubule regulation is a conserved feature of the Dis1/XMAP215 family of MAPs.

Introduction

Microtubules are intrinsically dynamic cytoskeletal structures. Rather than reaching a steady-state length, single microtubules switch stochastically between states of growth and shrinkage, and transitions between these states are known as catastrophe (growth to shrinkage) and rescue (shrinkage to growth), respectively. This dynamic instability allows quick reorganization of the microtubule cytoskeleton, such as from the interphase microtubule array to the mitotic spindle (for review see Desai and Mitchison, 1997).

Microtubule-associated proteins (MAPs) regulate microtubule dynamics. Some MAPs increase the net microtubule polymer mass (stabilizers), whereas others decrease it (destabilizers). As microtubules grow and shrink at ends, targeting to ends is considered an important feature of most MAPs (for review see Howard and Hyman, 2003). Three mechanisms of end targeting have been identified (for review see Carvalho et al., 2003; Galjart and Perez, 2003) and described as transport, hitchhiking, and direct end binding. A transported MAP binds a motor, which carries it to the end of a microtubule. For example, in *Saccharomyces cerevisiae*, Kar9 is transported to plus ends likely by associating with the kinesin motor Kip2 (Liakopoulos et al., 2003; Maekawa et al., 2003). A hitchhiking MAP is recruited to ends by interacting with another MAP already bound there. For example, the *S. cerevisiae* dynein homologue Dyn1 interacts with end-bound Bik1 and Pac1 (Lee et al., 2003; Sheeman et al., 2003). A direct end-binding MAP recognizes particular features of microtubule ends or copolymerizes with tubulin. Examples of direct end-binding MAPs are CLIP-170, mitotic centromere-associated kinesin (MCAK)/XKCM1, and members of the Dis1/XMAP215 family such as budding yeast Stu2p or human ch-TOG (Desai et al., 1999; Diamantopoulos et al., 1999; Perez et al., 1999; Spittle et al., 2000; Hunter et al., 2003; van Breugel et al., 2003).

Once at microtubule ends, MAPs influence microtubule dynamics by a still largely obscure mechanism. The best understood factors in this regard are members of the kinesin-13/MCAK family, which destabilize microtubules by inducing catastrophes. Kinesin-13 family members bind directly to microtubule ends and transform the end structure into one that is normally found in microtubules undergoing disassembly (Desai et al., 1999; Moores et al., 2002; Niederstrasser et al., 2002). A cycle of end binding, microtubule conformational change, and recycling of the MCAK family member requires the energy of ATP hydrolysis.

Less is known about end binding and microtubule regulation by microtubule stabilizers. The microtubule stabilizer XMAP215

J. Al-Bassam and M. van Breugel contributed equally to this paper.

Correspondence to Anthony Hyman: hyman@mpi-cbg.de

M. van Breugel's present address is Medical Research Council Laboratory of Molecular Biology, Cambridge CB2 2QH, United Kingdom.

Abbreviations used in this paper: MAP, microtubule-associated protein; MCAK, mitotic centromere-associated kinesin; NHS, *N*-hydroxysuccinimide; SPB, spindle pole body; TAP, tandem affinity purification.

The online version of this article contains supplemental material.

The Journal of Cell Biology, Vol. 172, No. 7, March 27, 2006 1009–1022
http://www.jcb.org/cgi/doi/10.1083/jcb.200511010

from *Xenopus laevis* increases microtubule growth rates in vitro. This property suggests that it could facilitate tubulin addition onto microtubule ends (Gard and Kirschner, 1987; Vasquez et al., 1994). There is only anecdotal evidence, however, that XMAP215 binds preferentially to ends, and a direct interaction with unpolymerized tubulin has not yet been described. Better evidence for such an assisted tubulin addition comes from work on the in vitro properties of ch-TOG, the human XMAP215 homologue (Charasse et al., 1998; Spittle et al., 2000). It is unclear, however, whether XMAP215 or ch-TOG stabilize microtubules by the same mechanism in vivo as they do in vitro. Indeed, XMAP215 apparently functions in vivo by opposing the catastrophe-promoting kinesin-13 member XKCM1 rather than by its direct influence on the microtubule growth rate (Tournebize et al., 2000; Kinoshita et al., 2001). An antagonistic relationship to the XKCM1 homologue MCAK has also been demonstrated for ch-TOG (Cassimeris and Morabito, 2004; Holmfeldt et al., 2004).

XMAP215 and ch-TOG are members of the Dis1/XMAP215 family. This is the only MAP family with representatives in fungi, plants, and animals. All of its members are essential for correct microtubule function during cell division (for review see Ohkura et al., 2001 and Kinoshita et al., 2002), but the individual Dis1/XMAP215 family proteins exhibit a puzzling diversity of functional properties. Most family members have a microtubule-stabilizing activity (Tournebize et al., 2000; Garcia et al., 2001; Nakaseko et al., 2001; Severin et al., 2001; Whittington et al., 2001; Gergely et al., 2003; Gräf et al., 2003; Cassimeris and Morabito, 2004; Holmfeldt et al., 2004), but they can also show destabilizing activity in some experimental contexts or can act to make microtubules more dynamic. Examples of the former are Stu2p (Usui et al., 2003; van Breugel et al., 2003), ch-TOG (Holmfeldt et al., 2004), and XMAP215 (Shirasu-Hiza et al., 2003); examples of the latter are Stu2p (Kosco et al., 2001) and msps, which acts as an antipause factor in vivo (Brittle and Ohkura, 2005). Conservation of primary structure among the Dis1/XMAP215 family members is variable and largely limited to the NH_2-terminal region, which contains two to five so-called TOG domains. The TOG domains, in turn, consist of degenerate HEAT repeats. Although HEAT repeats are generally described as protein interaction domains, the partners for these elements of Dis1/XMAP215 family members have yet to be identified (for review see Ohkura et al., 2001).

In this study, we report the results of experiments designed to identify functions for the TOG domains of the Dis1/XMAP215 family member Stu2p from budding yeast. We provide evidence that Stu2p stabilizes microtubules in vivo and that its TOG domains have crucial roles in this process. Stu2p has two TOG domains, which we designate TOG1 and TOG2 (Fig. 1 A). The region containing TOG1 interacts in vivo and in vitro with dimeric tubulin. Removal of this region does not affect the end-binding properties of Stu2p either in vivo or in vitro, but it leads to shortened microtubules in vivo. Thus, end binding and microtubule regulation by Stu2p in vivo are separable processes. We have complemented these observations with a biochemical characterization of the Stu2p domains and their role in the formation of a complex with free tubulin dimers. We show that a Stu2p dimer undergoes extensive conformational changes upon tubulin binding.

Our data support the following two-step picture for the mechanism of action of Stu2p in vivo. First, a Stu2p dimer forms a complex with a single tubulin heterodimer through contacts with its TOG1 domains. Second, this protein complex associates directly with microtubule plus ends, in part through the properties of TOG2 domains, where it facilitates the addition of tubulin to protofilaments at the microtubule ends. We propose that assisted plus end addition of tubulin, which is mediated by TOG domains, is the common function of Dis1/XMAP215 family MAPs.

Results

Dimerization of Stu2p enhances binding to microtubules

Stu2p is a dimer of 200 kD (De Wulf et al., 2003; van Breugel et al., 2003; see Table II and Fig. S3, available at http://www.jcb.org/cgi/content/full/jcb.200511010/DC1). To interpret any experiments in which domains of Stu2 were deleted, we first mapped the dimerization domain by coimmunoprecipitation experiments to the region between residues 599 and 774 (unpublished data), a segment that includes a predicted coiled coil (residues 658–761). We showed that this predicted coiled coil is indeed the dimerizing element by coexpressing differentially tagged forms of Stu2p and subsequent coimmunoprecipitation (Fig. 1, A and B). We demonstrated the importance of Stu2p dimerization in vivo using a strain in which endogenous Stu2p can be depleted by Cu^{2+} addition. In this strain, plasmid-expressed intact Stu2p compensated for the loss of endogenous Stu2p, whereas plasmid expression of Stu2p lacking the dimerization domain led to a growth defect (Fig. 1 C).

We also showed that the loss of dimerization substantially reduces Stu2p's affinity for microtubules. We coexpressed full-length HA-tagged Stu2p and myc-tagged Stu2p lacking the dimerization domain. To soluble extracts from these cells, we added increasing amounts of taxol-stabilized microtubules and separated microtubule-bound and unbound Stu2p by centrifugation. At ~3 μM of microtubules, 50% of full-length HA-Stu2p was bound, whereas even at ~33 μM of microtubules, binding of monomeric Stu2p-myc was less than half saturated (Fig. 1 D).

Role of the Stu2p TOG domains in microtubule binding and stabilization

Strains expressing truncated Stu2p lacking both TOG domains are not viable (unpublished data). Therefore, we focused on examining the effects of removing the NH_2-terminal first TOG domain (TOG1) in vivo. The following experiments show that TOG1 contributes to microtubule stabilization.

We determined mean microtubule lengths in a strain expressing Stu2 lacking TOG1 (Stu2-ΔTOG1) as exclusive Stu2 copy (Fig. 2, A and C). In early S phase arrested and released cells (Fig. 2 B), the removal of TOG1 resulted in a strong decrease in the mean lengths of both cytoplasmic microtubules and mitotic spindles compared with the intact Stu2 control (Fig. 2 D). We infer that the presence of TOG1 enhanced microtubule stability. As expected from this inference, the ΔTOG1 mutant has an increased sensitivity to the microtubule-destabilizing drug benomyl (Fig. 2 E). We tried to measure the in vivo dynamics

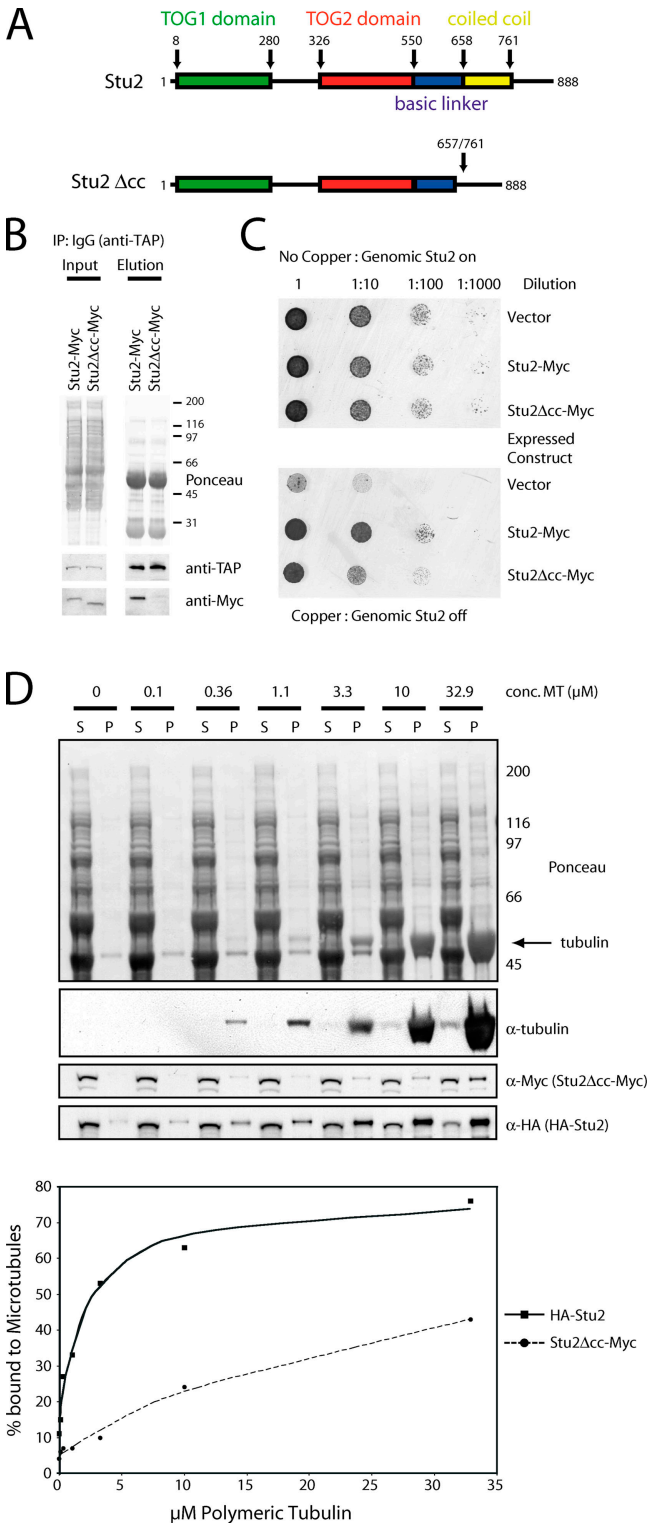

Figure 1. **Coiled-coil domain of Stu2p is required for homodimerization, affinity for microtubules, and the function of Stu2p in vivo.** (A) Scheme of Stu2p and the Stu2p mutant lacking the coiled-coil domain. Scheme shows the location of the first (green) and second TOG domain (red), basic linker domain (blue; previously termed the microtubule-binding domain), and the (predicted) coiled-coil domain (yellow). Boundaries of the TOG domains were determined from sequence alignments of Stu2p and Dis1/XMAP215 family members. Numbers indicate amino acid positions. (B) Immunoblot showing the results of a coimmunoprecipitation experiment. Stu2-myc or Stu2-myc lacking the coiled-coil domain (Stu2-Δcc–myc) was expressed in a yeast strain expressing Stu2-TAP. Stu2-TAP was immunoprecipitated from extracts, and the elutions were analyzed by SDS-PAGE and immunoblotting. (C) Stu2p function in vivo depends on the dimerization domain. Stu2-myc or Stu2–Δcoiled coil–myc (Stu2-Δcc–myc) was expressed in a yeast strain in which genomic Stu2p can be run down by adding copper. Strains were spotted in a dilution series on plates lacking or containing 300 μM $CuCl_2$. (D) Deletion of the coiled-coil segment reduces cosedimentation of Stu2p with microtubules. (top) Immunoblot showing a microtubule cosedimentation assay with yeast extracts. Yeast extracts from a strain expressing HA-Stu2 and Stu2-myc lacking the dimerization domain (Stu2-Δcc–myc) were incubated with increasing amounts of taxol-stabilized microtubules. Subsequently, the reactions were spun to separate microtubule bound from unbound proteins. Supernatants (S) and pellets (P) were analyzed by immunoblotting using anti-HA, anti-myc, and antitubulin antibodies. (bottom) Graph shows the percentage of bound HA-Stu2 and Stu2-Δcc–myc plotted against the concentration of polymerized tubulin incorporated into microtubules. For clarity, a curve has been fit to the data points.

of microtubules in the Stu2 mutant lacking TOG1, but we found that microtubules in the mutant were too short and short lived to be traced reliably (unpublished data).

Anaphase spindle elongation is a two-phase process in budding yeast (Kahana et al., 1995; Yeh et al., 1995; Straight et al., 1997). A first, fast phase driven by the Cin8 motor is followed by a slower phase driven by the Kip1 motor (Straight et al., 1998). We took time-lapse videos of spindle elongation in strains expressing GFP-tubulin and either intact Stu2 or Stu2-ΔTOG1 as the only source of Stu2p. Spindle lengths determined from projected images showed that the fast phase but not the slow phase was affected in the ΔTOG1 mutant (Fig. 3). The mean elongation rate in the fast phase was 0.57 μm/min (SD of 0.22 μm/min; $n = 15$) in the ΔTOG1 strain compared with 0.92 μm/min (SD of 0.16 μm/min; $n = 10$) in the intact Stu2 strain. The slow phase rates were essentially identical (0.25 and 0.23 μm/min, respectively; SD in both cases was 0.06 μm/min; $n = 15$ and $n = 10$, respectively; see Fig. S5 for details, available at http://www.jcb.org/cgi/content/full/jcb.200511010/DC1).

Stu2p associates with microtubule ends both in vivo and in vitro (He et al., 2001; Kosco et al., 2001; van Breugel et al., 2003; Tanaka et al., 2005). Analyzing strains expressing either Stu2-GFP or Stu2-ΔTOG1–GFP (Fig. 4 C) as exclusive Stu2 copies, we found by live cell imaging and indirect immunofluorescence that both forms localize correctly to microtubule ends (Fig. 4, A and B). Thus, destabilization of microtubules in the Stu2-ΔTOG1 mutant is not caused by a failure of the truncated protein to associate in vivo with microtubule ends. Using recombinant Stu2p and taxol-stabilized microtubules (see Materials and methods), we could likewise show that the deletion of TOG1 does not affect the direct association of Stu2p with microtubule ends in vitro (Fig. 4, D and E). However, the deletion of both TOG domains eliminates end binding in vitro (Fig. 4, D and E) and results in microtubule wall binding instead. Thus, in the absence of TOG1, Stu2p with only the TOG2 domain can still mediate end binding in vitro.

Because the deletion of TOG1 results in shortened microtubules and increased benomyl sensitivity, we tested whether increasing the number of TOG1 domains would lengthen microtubules and decrease benomyl sensitivity. Neither of these outcomes was observed. A strain with a doubled TOG1 domain of Stu2p does not have a lower sensitivity toward benomyl than the wild-type control (Fig. 5, A and B), nor is the mean length of cytoplasmic microtubules increased (unpublished data).

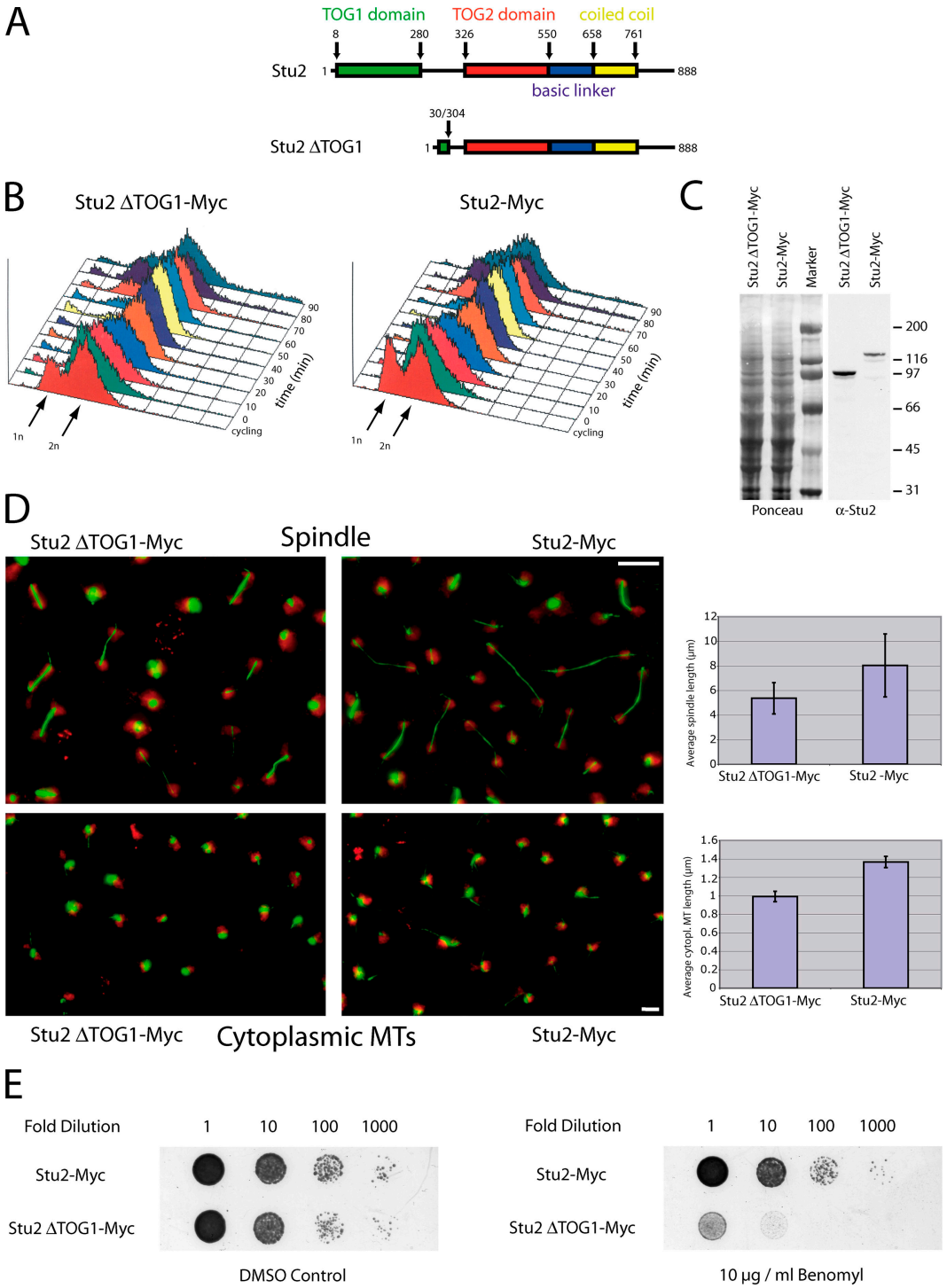

Figure 2. **The first TOG domain of Stu2p is required in vivo to stabilize both cytoplasmic and nuclear microtubules.** Stu2 or Stu2 lacking large parts of the first TOG domain (Stu2-ΔTOG1), both of which are COOH-terminally myc tagged, were expressed as exclusive Stu2 copies in yeast. The respective strains were arrested in early S phase with hydroxyurea and subsequently released from the hydroxyurea block, taking samples at 10-min time intervals for FACS and immunofluorescence analysis. Cytoplasmic microtubule lengths were determined from projected image stacks at time point zero; spindle lengths were determined from projected image stacks at the time points at which the peak of spindle elongation occurred. (A) Scheme of Stu2 and Stu2-ΔTOG1. See Fig. 1 A. (B) FACS profile of cultures before and during the hydroxyurea release. (C) Anti-Stu2p immunoblot of yeast extracts prepared from the cultures after the end of the hydroxyurea release. (D) Examples of antitubulin immunofluorescence of cytoplasmic microtubules at time point zero (bottom) and of microtubule spindles at the peak of spindle elongation (top). Tubulin, green; DNA, red. (right, bottom) Average cytoplasmic microtubule lengths (n = 590 for Stu2-myc and n = 366 for Stu2-ΔTOG1–myc). Error bars represent SEM. Bar, 2.5 μm. (right, top) Average microtubule spindle length (n = 195 for Stu2-myc and n = 178 for Stu2-ΔTOG1–myc). Error bars represent SD. Bar, 6 μm. Images have been processed using Photoshop, including some γ adjustments. (E) A yeast strain expressing an exclusive Stu2 copy of Stu2-ΔTOG1–myc shows enhanced sensitivity to the microtubule-destabilizing drug benomyl compared with a strain expressing intact Stu2-myc. Strains were spotted at the same cell densities onto YPD plates containing or lacking 10 μg/ml benomyl.

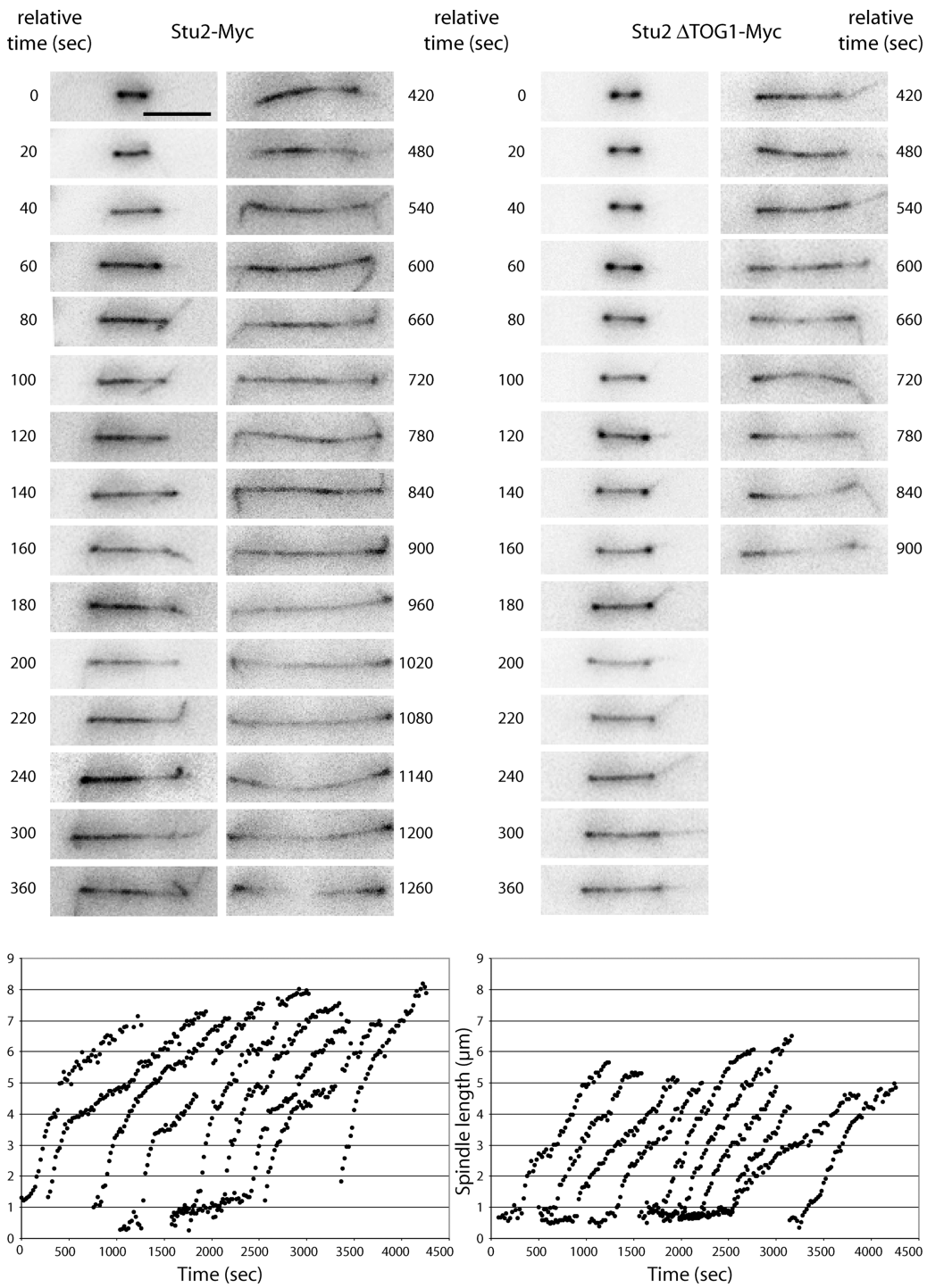

Figure 3. **The fast phase of anaphase spindle elongation is compromised by the deletion of TOG1.** (top) Still images of an elongating spindle, as followed by time-lapse microscopy, in cells expressing GFP-tubulin and either intact Stu2-myc (left) or Stu2-ΔTOG1–myc (right) as exclusive Stu2 copies. Bar, 3 μm. (bottom) Examples of traces of spindle lengths versus time. Individual traces have been shifted along the time axis to give clear spacing between them.

Role of TOG domains in binding free αβ-tubulin dimers

We used affinity chromatography to identify proteins that interact with the TOG domains of Stu2p (Fig. 6, A–C). Yeast extracts were run over columns carrying covalently immobilized recombinant TOG1, TOG2, or BSA. Bound proteins were eluted with high salt and analyzed by SDS-PAGE and Coomassie staining. One band was found specifically in the eluate of the TOG1 column that was not present in the eluate of the BSA or the TOG2 column (Fig. 6, A–C). This band was identified by immunoblotting (Fig. 6 C) and mass spectrometry (not depicted) as yeast tubulin. Thus, TOG1 but not TOG2 interacts tightly with tubulin heterodimer in vivo.

We expressed and purified recombinant TOG1, TOG1–TOG2, and full-length Stu2p to characterize their interaction with tubulin in vitro. TOG1–TOG2 is monomeric in solution, as shown

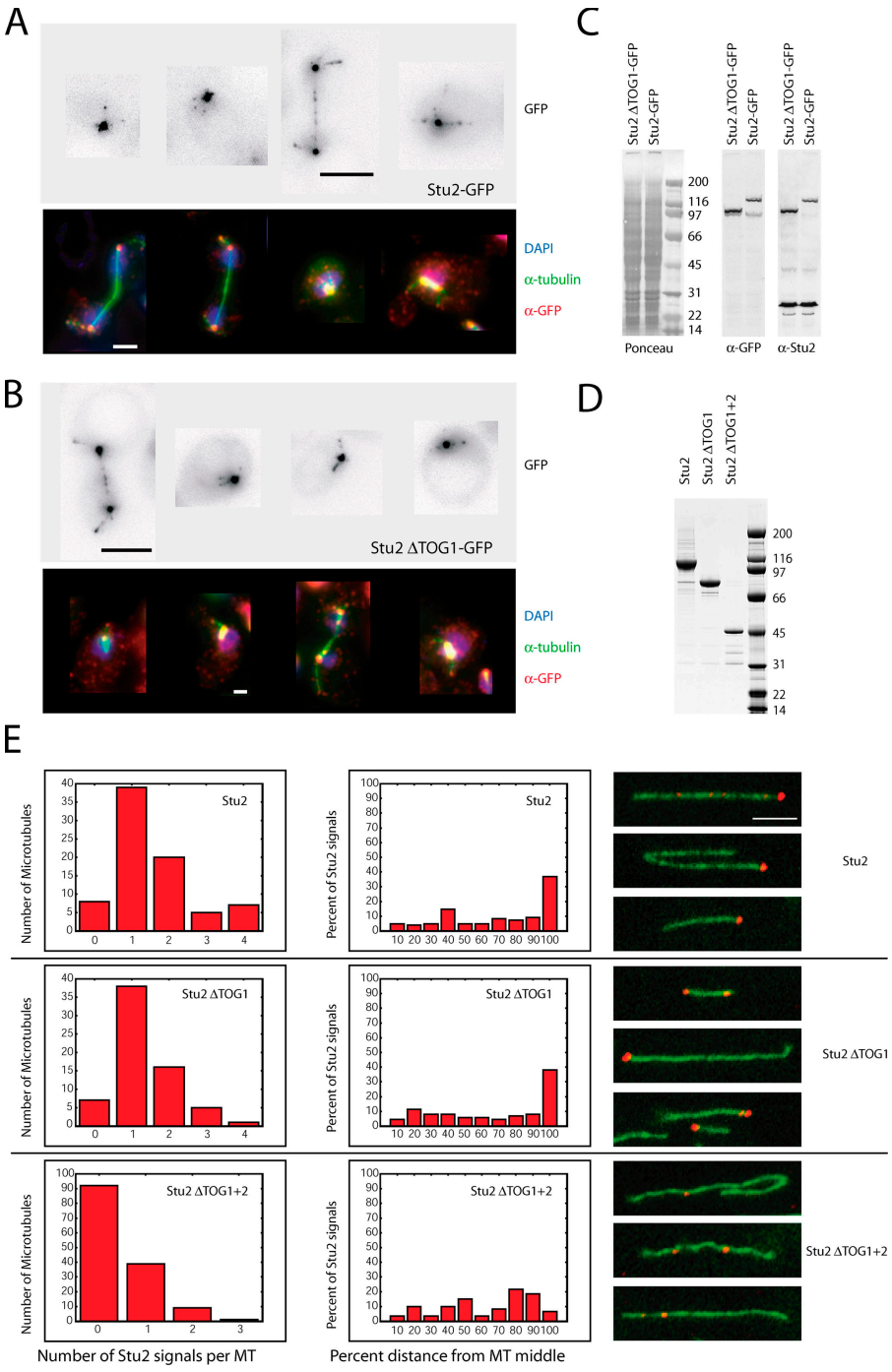

Figure 4. **The first TOG domain of Stu2p is not required for the end association of Stu2p.** (A and B) In vivo localization of Stu2-GFP and Stu2-ΔTOG1–GFP. (top) GFP localization was imaged directly from midlogarithmic yeast cultures expressing as exclusive Stu2 copies Stu2 (A) and Stu2-ΔTOG1 (B), which were both COOH-terminally GFP tagged. Bars, 5 μm. (bottom) Parts of the cultures were fixed and prepared for immunofluorescence imaging using anti-GFP and antitubulin (A, Stu2-GFP; B, Stu2-ΔTOG1–GFP). GFP, red; tubulin, green; DNA, blue. Images have been processed with Photoshop, including some γ adjustments. Bars (A), 2.2 μm; (B) 1.2 μm. (C) Anti-Stu2p and anti-GFP immunoblot of yeast extracts prepared from the yeast cultures used in A and B. (D) Coomassie-stained SDS-PAGE gel with equimolar amounts of the protein preparations used in E. (E) In vitro end-binding assay of Stu2p, Stu2p lacking the first TOG domain (Stu2-ΔTOG1), and Stu2p lacking both TOG domains (Stu2-ΔTOG1+2). Proteins were covalently labeled with Cy3 and incubated with taxol-stabilized microtubules partly labeled with Oregon green. Reactions were fixed, spun through a glycerol cushion, and resuspended before microscopic analysis. Fluorescence signals above 10% background level in the Cy3 channel were noted with their location along the microtubule. (left) Microtubule binding. The number of microtubules with a set number of Stu2 signals is displayed. (center) Microtubule end binding. Microtubules were divided in 10% intervals from the microtubule middle to the microtubule end, and the percentages of Stu2 signals found in each interval are displayed. (right) Three examples of microtubules with bound Stu2p fragments. Bar, 3 μm. Stu2 is in red, and microtubules are in green. For the purpose of this display only, images have been processed using Photoshop, including some γ adjustments.

by analytical ultracentrifugation (see Table II and Fig. S3). Its Stokes radius, estimated by size-exclusion chromatography (Table I), is larger than expected for isometric molecules of corresponding mass, indicating an elongated shape (Fig. 6, D and E). We mixed TOG1 and TOG1–TOG2 with tubulin dimers in 1:1 molar ratios and analyzed the mixture by size-exclusion chromatography (Fig. 6, D and E). Both fragments formed complexes with tubulin. We estimated the contents of tubulin and TOG construct in each of the peak fractions by SDS-PAGE and quantitative densitometry. Coomassie staining ratios of the peak fractions suggest that both TOG1 and TOG1–TOG2 bind to tubulin dimers with a stoichiometry of 1:1 (Fig. S2 C, available at http://www.jcb.org/cgi/content/full/jcb.200511010/DC1). When TOG1 and tubulin were mixed in a 2:1 stoichiometry, additionalTOG1 did not bind tubulin and eluted alone, suggesting that TOG1 does not bind tubulin in a stoichiometry higher than 1:1 (Fig. S2 D). We have observed similar effects with TOG1–TOG2 (unpublished data). The similarity of the apparent mass of the TOG1 or TOG1–TOG2–tubulin complexes to their expected masses suggests that rearrangement to a more globular shape accompanies tubulin binding (Table I). Electron microscopy of negatively stained preparations of the TOG1 and TOG1–TOG2 tubulin complexes supports this notion,

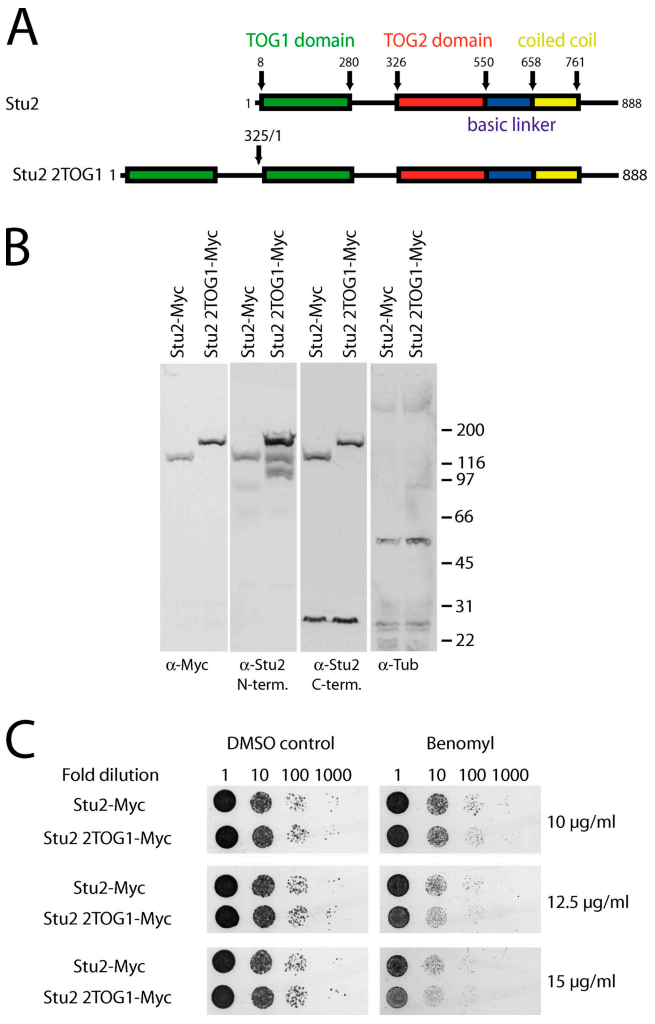

Figure 5. **Duplicating TOG1 of Stu2p does not hyperstabilize microtubules.** (A) Scheme of Stu2 and Stu2 with a duplicated first TOG domain (Stu2-2TOG1). See Fig. 1 A. (B) Immunoblot of yeast extracts prepared from cells expressing as exclusive Stu2 copies Stu2 or Stu2-2TOG1, which were both COOH-terminally myc tagged. Antibodies were anti-myc, anti-tubulin, an antibody raised against a COOH-terminal peptide of Stu2p, and an antibody raised against the NH_2 terminus (covering TOG1) of Stu2p. (C) Benomyl sensitivity test. Stu2 or Stu2-2TOG1, both COOH-terminally myc tagged, was expressed as exclusive Stu2 copies in yeast cells. Strains were spotted at the same cell densities onto YPD plates containing or lacking 10, 12.5, or 15 μg/ml of the microtubule-destabilizing drug benomyl.

showing globular particles, which are larger than free tubulin dimers (Fig. 7, B–E). Although the images of the particles are slightly heterogeneous, they are characterized by square shapes compared with the rectangular shape of the free tubulin dimer. Differences between the TOG1 and TOG1–TOG2 complexes were difficult to ascertain from the images. Although TOG1 and TOG1–TOG2 tubulin complexes remained intact on the time scale of the gel filtration experiment, they dissociated within hours after eluting from the column. This dissociation was also apparent in analytical ultracentrifugation experiments (unpublished data).

Dimeric Stu2p undergoes a conformational change while capturing one tubulin dimer

We confirmed by analytical ultracentrifugation that purified Stu2p is a dimer (Table II and Fig. S3), which is consistent with earlier studies (De Wulf et al., 2003; van Breugel et al., 2003). Its large apparent molecular mass and Stokes radius, like those of its fragments, indicate an elongated conformation in solution (Fig. 6 F and Table I). Indeed, electron microscopy of negatively stained preparations of Stu2p reveals elongated, string-like molecules of roughly constant width. Careful examination of the images suggests the presence of flexible joints (Fig. S4, available at http://www.jcb.org/cgi/content/full/jcb.200511010/DC1). The Stu2p molecules have an average contour length of 320 ± 35 Å and a width of ∼20–25 Å (Fig. 7 A and Fig. S4). Based on X-ray structures of other HEAT repeat–containing proteins, a single TOG domain, which consists of six HEAT repeats, should have a length of 65–70 Å and a thickness of 20–25 Å. Therefore, a dimer of TOG1–TOG2 should be ∼300 Å long. Our measurements of electron microscopy image dimensions are consistent with these estimates. The coiled coil and COOH-terminal extension, which we would expect to project from the midpoint of the molecular contour, were not detected, probably because they are too thin to exhibit contrast in negative stain.

When mixed in a 1:1 molar ratio with tubulin (two tubulin heterodimers per Stu2p dimer), Stu2p captured only about half of the tubulin added. SDS-PAGE and quantitative densitometry of the peak fractions from size-exclusion chromatography

Table I. **Hydrodynamic properties of Stu2p constructs and tubulin-bound complexes using size-exclusion chromatography**

Protein sample	Elution volume	Stokes radius[a]	Apparent mass[a]	Calculated mass
	(mL)	*(Å)*	*(kD)*	*(kD)*
αβ-tubulin dimer	16.1	43	∼110	100
TOG1	16.8	36	∼67	36
TOG1–TOG2	15.8	46	∼130	66
Stu2-ΔC (dimer)	13.2	79	∼765	182
Stu2p (dimer)	12.8	83	∼940	200
TOG1–tubulin	15.6	48	∼160	136
TOG1–TOG2–tubulin	15.2	52	∼195	167
Stu2-ΔC–tubulin	12.6	87	∼1,060	282
Stu2p–tubulin	12.2	92	∼1,340	300

[a]Apparent molecular masses and Stokes radii were calculated by determining the elution volumes of eight broad-range molecular weight standards of known mass and Stokes radius and were compared to their calculated mass. The Stokes radius for each sample was an average of the Porath and the Laurent and Killander Stokes radii, which corresponded closely.

Table II. **Molecular weight measurements of Stu2 constructs and Stu2-ΔC–tubulin complexes by sedimentation equilibrium analytical ultracentrifugation**

Stu2p construct	Computed mass	Measured mass
	(kD)	*(kD)*
Stu2p (wild-type dimer)	201	210 ± 8
TOG1–TOG2	66	67 ± 6
Stu2-ΔC (dimer)	182	168 ± 7
Stu2-ΔC–αβ-tubulin (2:1)	282	267 ± 13
Difference (αβ-tubulin)[a]	100	101[b]

[a]Difference between the fifth and sixth rows.
[b]The molecular weight of tubulin is the difference in mass between the measured molecular masses of the Stu2-ΔC–tubulin complex and Stu2-ΔC alone.

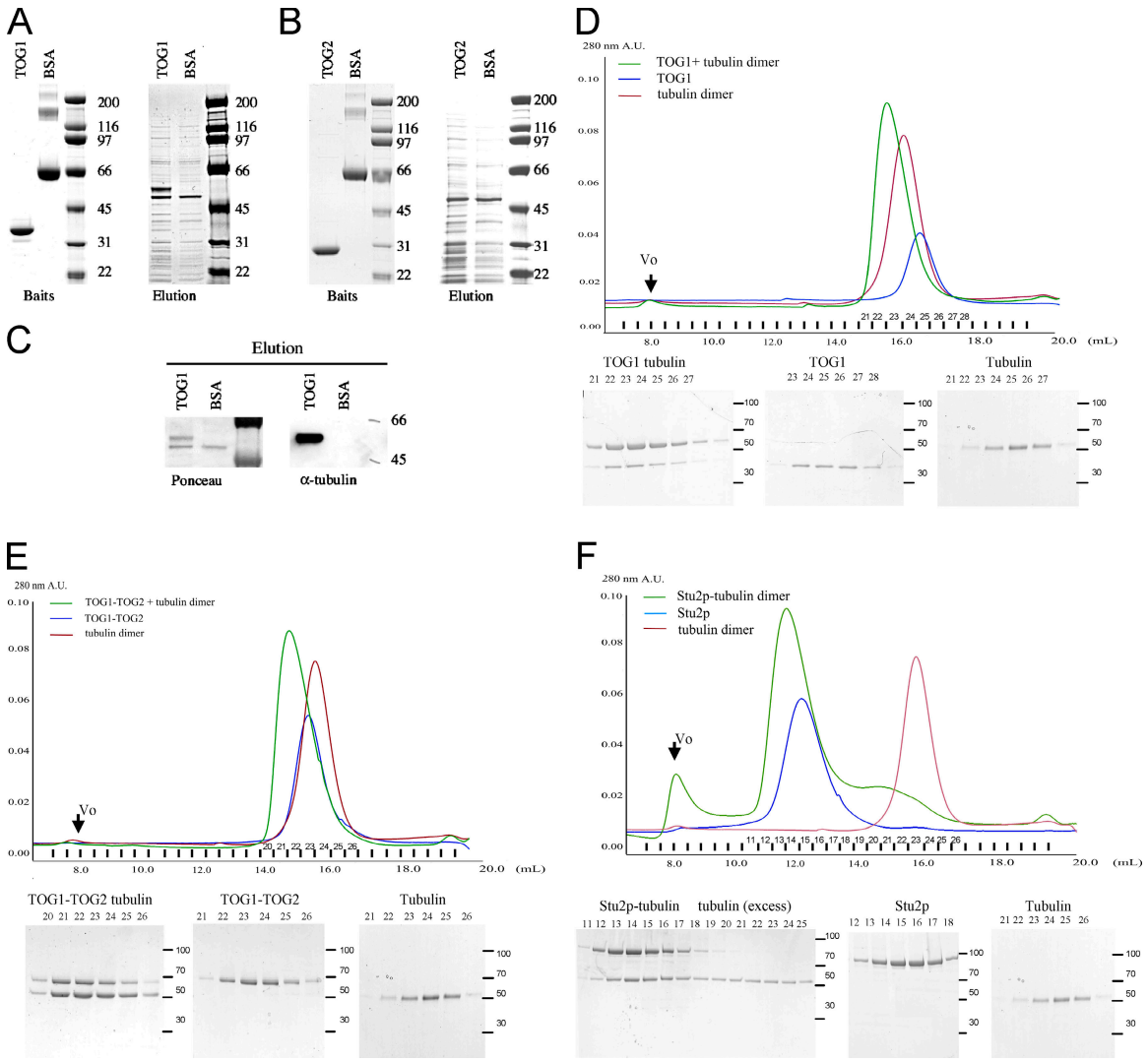

Figure 6. **Stu2p and its TOG1 domain fragment bind an αβ-tubulin heterodimer.** (A) Affinity chromatography using a recombinant first TOG domain of Stu2p (TOG1). 1.9 mg TOG1 or, as a control, 2.6 mg BSA were immobilized on NHS-activated columns (A, left; Coomassie-stained gel showing TOG1 and BSA before coupling to the column). Yeast extracts were prepared from a wild-type strain and passed through the column before washing and elution with high salt. Eluates were subjected to SDS-PAGE and the gel stained with Coomassie blue (A, right). The band present only in the elution of the column carrying TOG1 was identified by antitubulin immunoblotting (C) and mass spectrometry (not depicted) as yeast tubulin. (B) Affinity chromatography using a recombinant second TOG domain of Stu2p (TOG2). 2.2 mg TOG2 or, as a control, 2 mg BSA were immobilized on NHS-activated columns (left; Coomassie-stained gel showing TOG2 and BSA before coupling to the column). (C) Yeast extracts were prepared from a wild-type yeast strain and passed through the column carrying TOG1 before washing and elution with high salt. The eluates were subjected to SDS-PAGE, and the gel was stained with Coomassie (right) and antitubulin immunoblotting (left). (D) Size-exclusion chromatograms of recombinant TOG1 (blue) and unpolymerized αβ-tubulin dimer (red). Equimolar amounts of TOG1 and tubulin dimer were mixed and analyzed by gel filtration (green). SDS-PAGE of the peak fractions show that TOG1 coelutes with tubulins. The estimated stoichiometry is 1:1 for the TOG1/tubulin dimer from densitometry of the Coomassie blue–stained protein bands (Fig. S2 C, available at http://www.jcb.org/cgi/content/full/jcb.200511010/DC1). The elongated shape of TOG1 causes it to elute earlier than a globular protein of the same molecular weight (Table I). The unpolymerized αβ-tubulin chromatogram (red) and SDS-PAGE of fractions (bottom left) are also shown in E and F for comparison with other experiments. (E) Size exclusion chromatograms of recombinant TOG1–TOG2 (blue) and unpolymerized αβ-tubulin dimer (red). Equimolar amounts of TOG1–TOG2 and tubulin dimer were mixed and analyzed by gel filtration (green). SDS-PAGE of peak fractions shows that TOG1–TOG2 coelutes with tubulins. The estimated stoichiometry is 1:1 for the TOG1–TOG2/tubulin dimer (Fig. S2 C). Analytical ultracentrifugation shows that TOG1–TOG2 is a monomer with a molecular mass of 67 kD (Table II and Fig. S3), but its elongated shape causes it to elute earlier than a 67-kD globular protein (Table I). (F) Size-exclusion chromatograms of recombinant Stu2p (blue) and unpolymerized αβ-tubulin dimer (red). Equimolar amounts of Stu2p and tubulin dimer were mixed and analyzed by gel filtration (green). A complex forms with an apparent molecular mass slightly larger than that of free Stu2p, but excess, unbound tubulin is also detected. The Stu2p–tubulin complex contains one tubulin heterodimer per Stu2p homodimer (Fig. S2 C). Analytical ultracentrifugation shows that Stu2p is a dimer with a molecular mass of 200 kD (Table II and Fig. S3), but its elongated shape causes it to elute substantially earlier than expected for a protein of this size (Table I). (D–F) Arrows refer to the void volume of the size-exclusion column.

suggest that one tubulin heterodimer bound per Stu2p dimer (Fig. 6 F and Fig. S2 C). A large molecular weight aggregate containing only tubulin also formed (Fig. 6). This aggregate was not present when we added at least one Stu2p dimer per tubulin dimer (unpublished data). Unlike the complexes of tubulin with TOG1 and TOG1–TOG2, tubulin complexes with dimeric Stu2p were stable for many days after assembly. Deletion of the COOH-terminal segment (residues 773–888) distal to the coiled

coil to generate Stu2-ΔC did not affect the stoichiometry of the Stu2p–tubulin complex (Fig. S2, A and B). Deletion of the TOG1 domain (Stu2-ΔTOG1) interrupted the formation of a complex with tubulin (Fig. S2 E).

Complexes of full-length Stu2p with tubulin tend to aggregate over time; the Stu2-ΔC–tubulin complex does not. Therefore, we used analytical ultracentrifugation to determine the molecular mass of a dimeric Stu2-ΔC–tubulin complex after purification to confirm the tubulin binding stoichiometry (Table II and Fig. S3). The mass difference between Stu2-ΔC bound to tubulin (268 ± 13 kD) and Stu2-ΔC alone (167 ± 7 kD) was exactly equivalent to the mass of a single αβ-tubulin dimer (∼101 kD). The relative homogeneity in the mass of the Stu2-ΔC–tubulin complex shows that binding of homodimeric Stu2p to a single tubulin subunit is a tight stoichiometric interaction.

Electron microscopy of the negatively stained Stu2p–tubulin complex showed compact and relatively homogeneous structures ∼100 Å in diameter, although a few images of larger diameter were also evident (Fig. 7 E). Images of negatively stained Stu2-ΔC–tubulin complexes were very similar to those of complexes with the intact protein (Fig. S2 B), as expected from the absence of contrast from the COOH-terminal segment in images of free Stu2p. The circumference of the particles matches the average contour length of free Stu2p (320Å; Fig. 7 and Fig. S4). Thus, when it binds tubulin, the Stu2p dimer undergoes a transition from an extended conformation to a more compact one, perhaps encircling the captured tubulin dimer. The apparent variation in Stu2p–tubulin particle images is probably the result of deformation by negative stain, incomplete immersion in stain, and interaction with the carbon surface, as the molecular mass is homogenous (Table II and Fig. S3). Some of the variation may also reflect different views of the particle. The Stokes radius of the complex (92 Å) derived from size-exclusion chromatography is nonetheless larger than the apparent radius of the negatively stained complexes (∼50 Å) because of additional frictional drag from the projecting coiled coil and COOH-terminal segments not clearly contrasted by negative stain. The coiled coil alone should be ∼150 Å long and relatively stiff.

In summary, individual TOG1 or TOG1–TOG2 fragments bind a tubulin dimer reasonably tightly but dissociate fairly quickly. Intact Stu2p dimer binds a single tubulin heterodimer more strongly, with little or no dissociation during the time required for analytical ultracentrifugation experiments (several days). The two subunits of Stu2p dimer interact asymmetrically with the bound tubulin, which they encase compactly.

Discussion

In the experiments reported here, we have attempted to dissect the complex contributions of Stu2p to microtubule dynamics both in vivo and in vitro by examining the effects of altering one or more of its key structural elements and by studying the molecular properties of its complexes with tubulin. Our data assign a function to the evolutionally conserved TOG domains of the Dis1/XMAP215 family of MAPs and strongly suggest an in vivo mechanism of action for the budding yeast member of this family.

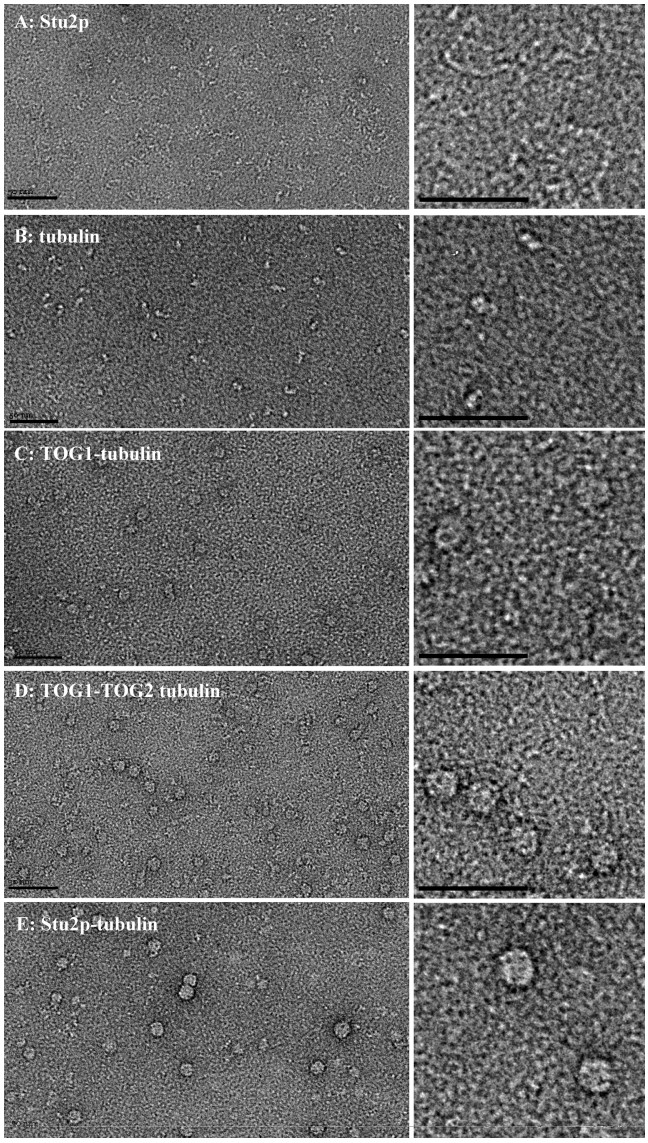

Figure 7. **Stu2p, an elongated flexible homodimer, forms a compact complex with αβ-tubulin heterodimer.** (A–E). Electron micrographs of negatively stained complexes obtained from the peak fractions illustrated in Fig. 6. The panels on the right are at twice the magnification of those on the left. Bars, 50 nm. (A) Stu2p homodimer. (B) Free αβ-tubulin heterodimer. (C) TOG1–tubulin complex. (D) TOG1–TOG2–tubulin complex. (E) Stu2p–tubulin complex. The uniform particles are slightly larger than those in the micrographs of TOG1–tubulin and TOG1–TOG2–tubulin.

Stu2p, like XMAP215, is an elongated molecule (Fig. 7; De Wulf et al., 2003; van Breugel et al., 2003). From the properties of Stu2p in solution and the images of negatively stained molecules in electron microscopy, we can picture it schematically, as shown in Fig. 8 A (top): a pair of TOG domain elements in each Stu2p subunit are connected through a linker to a dimerizing coiled-coil domain. The individual TOG domains, like other HEAT repeat–containing proteins, are probably stiff, but the segment between them may flex and so may the longer basic linker segment between TOG2 and the coiled coil. This linker was termed the microtubule-binding domain by Wang and Huffaker (1997). The basic linker is also found in Dis1 of *Schizosaccharomyces pombe* and was shown to be involved

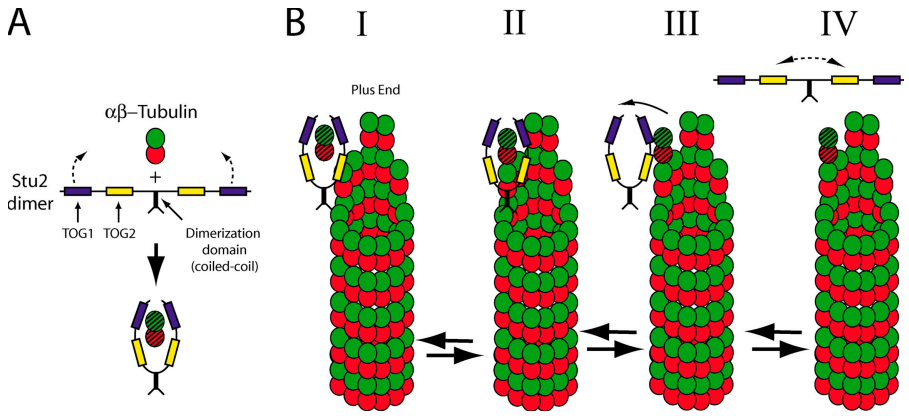

Figure 8. **Model for the mechanism of microtubule stabilization by Stu2p.** (A) A model for Stu2p dimer–tubulin dimer complex assembly. Stu2p dimer in extended conformation consisting of two tandem arrangements of TOG1 (purple) and TOG2 (yellow) held together by a coiled coil. Stu2p becomes compact when it sequesters a single tubulin heterodimer (crosshatched dimer). (B) Model of the loading of tubulin dimer to a microtubule plus end from a Stu2p dimer complex. (I) Stu2p–tubulin complex associates with microtubule plus ends through its TOG2 domains. (II) Stu2p positions its sequestered tubulin at the end of a single protofilament on the microtubule plus end. (III) Stu2p dissociates from the assembled tubulin dimer. (IV) Stu2p released from the microtubule plus end returns to its flexible conformation. The loading process of tubulin (I–IV) can become a tubulin removal process (IV back to I) if the equilibrium is reversed in the absence of dimeric tubulin, leading to microtubule depolymerization.

in microtubule binding (Nakaseko et al., 1996). However, the results in Fig. 4 show that it does not direct end-specific binding. We suggest that its strongly positive charge leads to an affinity for microtubule walls. Therefore, we have labeled this segment as basic linker in Figs. 1, 2, and 4 and Fig. S1 (available at http://www.jcb.org/cgi/content/full/jcb.200511010/DC1); its sequence is not conserved among homologous proteins from other fungi.

Stu2p binds microtubules (Wang and Huffaker, 1997), associating preferentially with microtubule ends (He et al., 2001; Kosco et al., 2001; van Breugel et al., 2003; Tanaka et al., 2005). The data shown here suggest that TOG1 contributes to microtubule stability in vivo, as the removal of TOG1 decreases microtubule length without affecting end association (Fig. 4). This result also implies that Stu2p end association is not strictly coupled to the stabilization of microtubules. The mechanism by which Stu2p alters microtubule dynamics in cells is, therefore, likely to be more complex than simple end capping or distortion of the microtubule end structure.

How, then, does Stu2p stabilize microtubules? The mechanism may be related to our observation that Stu2p sequesters free tubulin in vitro. The open, flexible Stu2p dimer undergoes a substantial compaction when it binds tubulin, and the simplest interpretation of the electron microscopy images is that its two "wings" collapse or wrap around a single αβ-tubulin heterodimer (Fig. 8 A, bottom). The length of the TOG regions of Stu2p particle electron microscopy images (~320 Å) matches the circumference of Stu2p–tubulin complexes (~315 Å). Full affinity and a well-defined structure depend both on the two TOG domains and on Stu2p dimerization. TOG1 probably mediates the interaction with tubulin; monomeric TOG1 and TOG1–TOG2 bind tubulin dimers tightly, but TOG2 alone does not (Fig. 6). The central role of TOG1 in tubulin binding in vitro and microtubule stabilization in vivo thus suggests that both activities might be linked.

A recent in vivo imaging study (Tanaka et al., 2005) suggested that Stu2p can be transported toward the plus end. The arrival of Stu2p at an end coincides with a microtubule rescue event (i.e., transition from shrinkage to growth). After reaching their maximum length, microtubules subsequently shrink, and the Stu2p signal slowly fades, presumably as the molecule diffuses away from microtubule ends. Combining these observations with the results reported in this study, we propose the following model for the mechanism of Stu2p action (Fig. 8). We envisage that Stu2p captures a tubulin heterodimer in the cell through its two sets of TOG domains, which are linked by the dimerizing coiled coil (Fig. 8 A). Once transported to microtubule plus ends, Stu2p might associate directly with the microtubule, at least in part, through one or both TOG2 domains in the Stu2p–tubulin complex (Fig. 8 B, I). Stu2p could then position its bound tubulin heterodimer at the plus end of a protofilament (Fig. 8 B, II), dissociate from that dimer, and return to its open conformation (Fig. 8 B, III– I V). This active tubulin-loading process could enhance tubulin assembly at growing plus ends or rescue shrinking ends. It could be part of a mechanism of microtubule rescue observed in vivo. The two activities of Stu2p, microtubule end binding and tubulin dimer sequestration, which are linked to the full assembly of TOG1 and TOG2 domains in the context of the Stu2p dimer, may well account for the complexities of its effects on microtubule dynamics under different circumstances in vivo and in vitro (Kosco et al., 2001; Severin et al., 2001; Usui et al., 2003; van Breugel et al., 2003).

Stu2p dimerization through its coiled coil is necessary for its correct function. Deletion of the coiled coil leads to a growth defect in vivo (Fig. 1, B and C) and produces defects in microtubule binding in vitro (Fig. 1 D). Our in vitro results also show that monomeric Stu2p would not retain its bound tubulin dimer tightly enough for reliable delivery to microtubule plus ends, and both TOG2 domains of a Stu2p dimer may also be necessary for stable plus end association (Fig. 8).

In contrast to its apparent activity in vivo, Stu2p destabilizes microtubules in vitro (van Breugel et al., 2003). This destabilization correlates with end binding, as only Stu2p fragments

that associate preferentially with microtubule ends are able to destabilize microtubules (unpublished data). Why are the in vitro and in vivo effects of Stu2p on microtubule stability different? One explanation might be that under the in vitro conditions used for stability assays, Stu2p has an altered affinity for a reaction intermediate at microtubule ends, driving the equilibrium toward destabilization in vitro and stabilization in vivo (Fig. 8 B, reverse arrows from III to I). For example, a higher affinity for free tubulin in vitro than in vivo could pull tubulin from microtubule ends rather than add it to them. A similar mechanism might explain why the microtubule-stabilizing Stu2p homologue XMAP215 can act in vitro as a destabilizer as well (Shirasu-Hiza et al., 2003). Finally, posttranslational modifications might account for differences in the observed activities. We found that Stu2p is multiply phosphorylated in vivo and that this phosphorylation changes in a cell cycle–dependent manner (unpublished data).

A symmetric Stu2p dimer associates with an asymmetric tubulin heterodimer. The two Stu2p subunits must recognize different tubulin surfaces, and one contact could be substantially stronger than the other. The TOG2 region, which does not interact strongly with tubulin dimers but plays a structural role in the complex, might recognize protofilament ends on its own. We have not yet been able to capture the end-bound state by electron microscopy. Homologues of Stu2p like XMAP215 and DdCP224 are monomers (Gard and Kirschner, 1987; Gräf et al., 2000; Cassimeris et al., 2001) and lack the dimerizing coiled-coil domain, but they contain three more TOG domain segments (five in XMAP215 and DdCP224; for review see Ohkura et al., 2001). The first two of these TOG domains have weak sequence similarities with TOG1 and TOG2, respectively (Gard et al. 2004), and the differential function of the two domains in binding free tubulin dimers and microtubule ends, respectively, may be preserved in the longer XMAP215 and ch-TOG proteins. The property conferred to Stu2p by dimerization may be mimicked in the monomeric homologues by differentiation among the additional TOG domains in those proteins.

Materials and methods

Cloning of the Stu2 constructs

The starting plasmid for in vivo Stu2p constructs was a gift of T. Huffaker (Cornell University, Ithaca, NY) and carried (under its own promoter region) full-length Stu2 COOH-terminally tagged with HA (parent pRS315). A HindIII restriction site in the upstream promoter region was removed by ApaI cleavage, and the vector was religated. Stu2 was removed from the vector by cleavage with HindIII–SphI (cutting at 84–88 bp within the coding region and downstream of the stop codon, respectively), and the corresponding Stu2 constructs were reintroduced into the HindIII–SphI sites. The Stu2 fragments were cloned as HindIII–EcoRI pieces lacking a stop codon and ligated together with an EcoRI–SphI piece carrying the myc_9 or EGFP tag followed by a stop codon. For the cloning of Stu2 carrying an extra first TOG domain, the parent vector was cut with HindIII (cutting at codon 29), and a three-way ligation was performed using a HindIII–XhoI piece from codon 29–325 (end of the spacer between TOG1 and TOG2) and a XhoI–HindIII piece from codon 1–29. For the cloning of Stu2 lacking the coiled-coil domain, a four-way ligation was performed using a HindIII–XmaI piece from codon 29–657 (last codon of basic linker; previously termed microtubule-binding domain by Wang and Huffaker, 1997), a codon before the start of the coiled-coil domain, an XmaI–EcoRI piece from codon 761 (last codon of the coiled coil)–888 (last codon before the stop), and an EcoRI–SphI piece carrying the myc_9 tag followed by a stop codon. In vivo constructs used in this study are also shown in Fig. S1: Stu2 (residues 1–888), Stu2-ΔTOG1 (residues 1–30 and 304–888), Stu2-2TOG1 (residues 1–325-LE-1-888), and Stu2–Δcoiled coil (residues 1–657-PG-761-888).

In vitro constructs used in this study are also outlined in Fig. S1 and included: Stu2p (residues 1–888), Stu2-ΔTOG1 (residues 266–888), Stu2-ΔTOG1+2 (residues 551–888), Stu2-ΔC (residues 1–772), TOG1–TOG2 (residues 1–587), TOG1 (residues 1–306 or residues 1–317 for gel filtration and electron microscopy), and TOG2 (residues 307–550). Stu2-ΔTOG1 or Stu2-ΔTOG1+2 were prepared by cloning the corresponding coding sequences as an NcoI–XhoI fragment into pFASTBac HTa (Invitrogen). Sequences corresponding to TOG1 and TOG2 were cloned as EcoRI–XhoI pieces into pGEX-6P-1 in frame with an NH_2-terminal GST tag. Sequences of TOG1 and TOG1–TOG2 were also cloned in pET28a using NcoI–XhoI fragments in frame with a COOH-terminal His tag (Table III).

Protein expression and purification

Baculoviruses expressing wild-type Stu2p, Stu2p-ΔTOG1, or Stu2p-ΔTOG1+2 were generated by transforming corresponding transfer vectors into the DH10bac *Escherichia coli* strain. Bacmids were prepared and transfected into *Spodoptera frugiperda* cells according to standard procedures. Recombinant baculoviruses were amplified three times before the large-scale infection of SF+ cells. Wild-type Stu2p was purified as previously described (Stu2 baculovirus was a gift of P. Sorger, Massachusetts Institute of Technology, Cambridge, MA; van Breugel et al., 2003) or by using Ni–nitrilotriacetic acid (NTA) chromatography followed by gel filtration using a Superdex-200 column and by ion exchange chromatography using a Hitrap-SP column (GE Healthcare). Insect cell–expressed Stu2p-ΔTOG1 and Stu2p-ΔTOG1+2 were prepared by successive steps of ammonium sulfate precipitation, metal affinity chromatography using Talon resin (CLONTECH Laboratories, Inc.), and ion exchange chromatography using a 1-ml Mono-S column (GE Healthcare) followed by gel filtration on a Superose 6 column run in BRB80 (80 mM Pipes, pH 6.8, 1 mM EGTA, and 1 mM $MgCl_2$), 100 mM KCl, 0.25% Brij-35, 5% glycerol, and 1 mM DTT.

TOG1, TOG1, and TOG1–TOG2 protein were expressed in BL21 (DE3) codon+ RIL cells (Stratagene). Cultures were grown at 29°C in LB to

Table III. **Yeast strains used in this study**

Strain	Strain description	Strain source
TH 1018	W303, Stu2del::Trp, GFP-Tub1::His, pRS315 carrying Stu2-myc(9) under endogenous Stu2p promoter region	This study
TH 1019	W303, Stu2del::Trp, GFP-Tub1::His, pRS315 carrying Stu2-ΔTOG1–myc(9) under endogenous Stu2p promoter region	This study
TH 1022	W303, Stu2del::Trp, GFP-Tub1::His, pRS315 carrying Stu2-2TOG1–myc(9) under endogenous Stu2p promoter region	This study
TH 1023	W303, Stu2del::Trp, pRS315 carrying Stu2-GFP under endogenous Stu2p promoter region	This study
TH 1024	W303, Stu2del::Trp, pRS315 carrying Stu2-ΔTOG1–GFP under endogenous Stu2p promoter region	This study
TH 1026	W303, Stu2-TAP-Trp, pRS315 carrying Stu2-myc(9) under endogenous Stu2p promoter region	This study
TH 1027	W303, Stu2-TAP-Trp, pRS315 carrying Stu2–Δcoiled coil–myc(9) under endogenous Stu2p promoter region	This study
TH 1028	CUY1147 (Kosco et al., 2001), Leu del::Trp, pRS315 carrying Stu2-myc(9) under endogenous Stu2p promoter region	This study
TH 1029	CUY1147 (Kosco et al., 2001), Leu del::Trp, pRS315 carrying Stu2–Δcoiled coil–myc(9) under endogenous Stu2p promoter region	This study
TH 1030	CUY1147 (Kosco et al., 2001), Leu del::Trp, pRS315	This study

0.5–0.6 OD and induced either for 2–3 h with 0.1–0.3 mM IPTG at 29°C or induced at 16°C for 5 h with 0.2 mM IPTG. Cells were harvested by centrifugation and cold lysis buffer (10 mM K-Pipes, pH 6.8, 1 mM $MgCl_2$, 3 mM EGTA, 0.25% Brij-35, 5% glycerol, 500 mM KCl, 2 mM EDTA, and 1 mM DTT). Lysis buffer was supplemented with complete protease inhibitor tablets (Roche), and lysozyme (Sigma-Aldrich) was added to the pellets followed by resuspension. The solution was sonicated using a sonicator (450-D; Branson) for several cycles. Lysates were spun at 70 krpm on a rotor (MLA80; Beckman Coulter) for 10 min at 4°C, and the supernatants were incubated with either 2–3 ml of lysis buffer–equilibrated glutathione–Sepharose beads (GE Healthcare) for GST-tagged constructs or with 4–5 ml Ni-NTA resin (QIAGEN) for His-tagged constructs. For GST-tagged constructs, the glutathione beads were incubated at 4°C for 1 h and were washed with lysis buffer and with precision cleavage buffer (50 mM Hepes, pH 7.5, 150 mM NaCl, 1 mM EDTA, 1 mM DTT, and 0.01% Tween-20). The glutathione beads were then mixed with 150–250 μl GST-tagged precision protease (a gift of D. Drechsel, Max Planck Institute of Molecular Cell Biology and Genetics, Dresden, Germany). Cleavage was performed for 8–16 h at 4°C. The bead solutions were spun through a frit, and the flow-through fractions containing cleaved protein were collected. His-tagged proteins were purified from Ni resin by washing with wash buffer (50 mM Tris, 250 mM NaCl, pH 7.5, and 5 mM β-mercaptoethanol) and were eluted with elution buffer (wash buffer + 320 mM imdazole) in 1-ml fractions. Fractions were evaluated by SDS-PAGE, and aliquots were snap frozen in liquid nitrogen.

Stu2p antibodies

The NH_2-terminal Stu2p antibody was raised against Stu2p-TOG1 (aa 1–306) by Elevage Scientific des Dombes. The COOH-terminal Stu2p antibody was raised against a COOH-terminal peptide of Stu2p (Eurogentec). Both antibodies were affinity purified.

FACS analysis

FACScan was used as described previously (Epstein and Cross, 1992).

Immunoprecipitations

Strains expressing tandem affinity purification (TAP)–tagged Stu2p together with myc-tagged Stu2p or myc-tagged Stu2p–Δcoiled coil were grown in synthetic medium (synthetic drop-out media [−Leu] containing 2% glucose) to midlogarithmic phase and were harvested by centrifugation. Lysis buffer BRB80 (80 mM Pipes, pH 6.8, 1 mM EGTA, and 1 mM $MgCl_2$), 5% glycerol, 100 mM KCl, 0.25% Brij-35, and 2 mM DTT supplemented with complete protease inhibitor tablets (Roche) was added 1:1 (vol/vol), and cells were lysed by bead beating. Lysates were spun three times (2 min at 14 krpm, 5 min at 100 krpm, and 2 min at 14krpm; all at 4°C), and 150 μl of cleared lysates were added to 10 μl of equilibrated IgG Sepharose 6 Fast Flow slurry (GE Healthcare). Reactions were incubated on a rotating wheel for 1 h at 4°C. After six 0.2-ml washes with lysis buffer, beads were eluted with laemmli buffer. Eluates were analyzed by immunoblotting using an excess of rabbit antibody (to block protein A of the TAP tag) and the anti-myc antibody 9E10. After stripping of the blot, protein A detection reagent (Sigma-Aldrich) was used to detect the TAP tag.

Microtubule binding of Stu2p and Stu2p–Δcoiled coil

Yeast strain TH1029 expressing HA-tagged Stu2p and myc-tagged Stu2p–Δcoiled coil was grown in synthetic medium (synthetic drop-out media [−Leu] containing 2% glucose) to midlogarithmic phase. Cells were harvested by centrifugation. Lysis buffer supplemented with 20 μM taxol was added 1:1 (vol/vol), and cells were lysed by bead beating. Lysates were cleared twice by centrifugation (5 min at 100 krpm and 4°C) and were respun (14 krpm for 10 min at 4°C). The protein concentration was 18 mg /ml. 5 μl taxol-stabilized microtubules were added to 20 μl of the supernatants (0–32.9-μM final concentrations). Reactions were incubated for 7 min on ice, and 20 μl were spun for 10 min at 70 krpm through a 50-μl glycerol cushion (50% in BRB80) in TLA100 tubes (Beckman Coulter) at 4°C. Equivalent amounts of supernatants and pellets were separated by SDS-PAGE followed by immunoblotting using the anti-myc antibody 9E10, the antitubulin antibody DM1α (Sigma-Aldrich), and a polyclonal anti-HA antibody (Santa Cruz Biotechnology, Inc.). Blot quantification was performed using the plot profile function of Image 1.62a software (Scion). A best-fit curve was created only for optical display using the data points and the function $y = y_0 + (Bmax - y_0) \times x/(Kd + x)$, where x = the concentration of microtubules, y = the percent binding of Stu2p, y_0 = the percent binding of Stu2p at x = 0, Bmax = the percent binding of Stu2p at $x = \infty$, and Kd = the dissociation constant. Bmax, y_0, and Kd were determined from the fit.

Measurement of spindle and cytoplasmic microtubule length in vivo

Cells were grown at 30°C in YPD to an OD_{600} of 0.4 in a 50-ml culture and were arrested in early S phase by the addition of 0.6 g hydroxyurea for 3.5 h. Cells were washed twice with 50 ml YPD by centrifugation and released at 30°C by resuspension in 50 ml YPD. Samples were taken at 10-min intervals for immunofluorescence and FACS analysis. The remainder of the culture was used for extract preparation and immunoblotting. For immunofluorescence, cells were fixed with formaldehyde and processed according to standard yeast techniques. Antibodies were monoclonal antitubulin antibody DM1α (Sigma-Aldrich) and a directly Cy3-labeled anti–mouse antibody (Jackson ImmunoResearch Laboratories). DNA was visualized using DAPI. Imaging of immunofluorescence was performed using a 100× NA 1.35 objective on a microscope (DeltaVision; Olympus) using SoftWorx (Applied Precision) and taking stacks (30 images with 0.2-μm z spacing) for each field using a camera (CoolSNAP HQ; Roper Scientific). Cytoplasmic microtubule lengths were measured from projected images from the microtubule tip to the spindle pole body (SPB) as multiple segments (SoftWorx), taking the samples from time point zero. The average cytoplasmic microtubule length for Stu2-ΔTOG1–myc was 0.99 ± 0.06 μm (±SEM; $\alpha = 0.05$; $n = 366$) and for Stu2-myc was 1.37 ± 0.06 μm (±SEM; $\alpha = 0.05$; $n = 590$). Spindle lengths were measured as multiple segments along elongated spindles from SPB to SPB using projected images of the time points at which the peak of spindle elongation frequency occurred (50–70 and 50–80 min after release for Stu2-myc and Stu2-ΔTOG1–myc, respectively). Elongated spindles were defined as those along which the DNA masses were completely segregated as judged by DAPI staining. The average spindle length for Stu2-ΔTOG1–myc was 5.36 ± 1.27 μm (±SD; $n = 178$) and for Stu2-myc was 8.03 ± 2.56 μm (±SD; $n = 195$). Images depicted in this paper were projected using SoftWorx and were processed using Adobe Photoshop.

Benomyl sensitivity test of yeast strains

5 μl of yeast cultures were spotted at the same OD_{600} and in serial dilutions of 1:10, 1:100, and 1:1,000 on YPD plates containing 10, 12.5, or 15 μg/ml benomyl or on the DMSO control plates. The plates were subsequently incubated at 30°C for the same amount of time.

Measurement of spindle elongation kinetics

Agar pads were prepared using molten synthetic drop-out media (−Leu) containing 2% glucose and agar and depression slides. 4 μl of midlogarithmic yeast cultures concentrated by centrifugation (at 3 krpm for 20–40 s at room temperature) were deposited onto the pads, which were then covered by 25 × 25-mm coverslips, and the edges were sealed with Vacuum Grease (Beckman Coulter). Imaging was performed using a 100× NA 1.35 objective with a slightly closed numeric aperture ring on a microscope (DeltaVision; Olympus) using SoftWorx. Stacks (five images with 0.6-μm z spacing) were taken for each time point with a 0.2-s exposure per image; 100 stacks were recorded with a camera (CoolSNAP HQ; Roper Scientific) with a time lapse between stacks of 20 s. The temperature as measured by a thermometer attached to the stage ranged from 24.5 to 25.8°C. Spindle lengths were measured from projected stacks using multiple segments along the spindles (SoftWorx) from SPB to SPB. In case of unclear SPB position, no spindle length for this time point was measured. Spindle average elongation speed was calculated from the start of elongation to a visible drop in the elongation speed (fast phase) and from this point to the end of spindle elongation (slow phase). If no drop in elongation speed could be assigned, the total speed of spindle elongation was taken for both the fast and the slow phase. Average fast spindle elongation speeds for Stu2-myc was 0.92 ± 0.16 μm/min (±SD; $n = 10$) and for Stu2-ΔTOG1–myc was 0.57 ± 0.22 μm/min (±SD; $n = 15$). The slow spindle elongation speed for Stu2-myc was 0.23 ± 0.06 μm/min (±SD; $n = 10$) and for Stu2-ΔTOG1–myc was 0.25 ± 0.06 μm/min (±SD; $n = 15$). Images were processed using Photoshop.

Visualization of Stu2p end association in vivo

1 ml of midlogarithmic yeast culture was concentrated by brief centrifugation and directly imaged in the GFP channel using a microscope (DeltaVision; Olympus) as described below. Another 1 ml of the culture was fixed using a formaldehyde/PFA mixture and processed for immunofluorescence using standard yeast techniques. Antibodies were a sheep anti-GFP antibody (Neef et al. 2003), DM1α mouse antitubulin antibody (Sigma-Aldrich), and directly labeled secondary antibodies (AlexaFluor594-labeled donkey anti–sheep; Invitrogen) or FITC-labeled donkey anti–mouse (Jackson ImmunoResearch Laboratories). DNA was visualized with DAPI. Imaging was performed using a 100× NA 1.35 objective on a DeltaVision microscope using SoftWorx. Stacks (30 images with 0.2-μm z spacing)

were taken for each field using a camera (CoolSNAP HQ; Roper Scientific). Images were projected using SoftWorx and processed using Photoshop. The remainders of the cultures were used for extract preparation and immunoblotting using a polyclonal goat anti-GFP antibody (gift of D. Drechsel).

Visualization of Stu2p binding to microtubules in vitro

20 nM of prespun (at 100 krpm for 5 min at 4°C in a TLA100 rotor) directly Cy3-labeled Stu2p or Stu2p fragments (Stu2-ΔTOG1 or Stu2-ΔTOG1+2) in BRB80, 5% glycerol, 100 mM KCl, 0.25% Brij-35, 1 mM DTT, and 20 μM taxol, pH 6.8, were incubated for 5 min at room temperature with 25 μM taxol-stabilized partly Oregon green–labeled microtubules. The reactions were fixed with 1.5% glutaraldehyde for 5 min, quenched for 5 min with 0.1% sodium borohydride, and spun through a 40% glycerol (in BRB80) cushion for 10 min at 25°C in a TLA100 rotor at 70 krpm. Pelleted microtubules were subsequently resuspended in BRB80, 5% glycerol, 100 mM KCl, 0.25% Brij-35, 1 mM DTT, and 5 μM taxol, pH 6.8, before microscopic analysis. Images were acquired using a microscope (Axioplan 2; Carl Zeiss MicroImaging, Inc.) with a 63× N.A. 1.40 plan-Apochromat lens (Carl Zeiss MicroImaging, Inc.) together with the MetaMorph Imaging System (version 1.4.2; Molecular Devices) using a camera (Orca-ER; Hamamatsu). The intensities of the signals in the Cy3 (labeled Stu2p and Stu2p fragment) channel were scanned along the length of microtubules using the linescan function of the MetaMorph Imaging software with a pixel width of five. Peaks higher than 10% of the median intensity along the microtubule were scored with their location along the microtubule. Microtubules were divided in 10% intervals from the microtubule middle to the microtubule ends. 67 (Stu2-ΔTOG1), 79 (Stu2), and 141 (Stu2-ΔTOG1+2) microtubules were analyzed. Images were processed using PhotoShop.

In this assay, *E.coli*–derived Stu2-ΔTOG1 but not *E.coli*–derived Stu2-ΔTOG1+2 behaved differently from the insect cell–derived equivalent protein used in this study. In contrast to insect cell–derived Stu2-ΔTOG1, *E.coli*–derived Stu2-ΔTOG1 shows no preferential end binding but binds laterally along the microtubules and behaves differently in a sucrose gradient and in size-exclusion chromatography. As *E. coli*–derived full-length Stu2 could not be made, we assume that *E.coli*–derived Stu2-ΔTOG1 is improperly folded. Thus, for consistency, the in vitro end-binding analysis presented in this study has been based on insect cell–derived proteins.

Affinity chromatography

Recombinant protein was immobilized on a 1-ml *N*-hydroxysuccinimide (NHS)–activated HiTrap column according to standard procedures (GE Healthcare). Yeast extracts were prepared from a haploid W303 strain. Cultures were grown in YPD at 30°C to ~1.0 OD_{600}, spun, and pellets were washed twice with cold H_2O and weighed. 1 vol/wt of ice-cold lysis buffer was added (100 mM K-Hepes, 50 mM NaF, 50 mM β-glycerophosphate, 10 mM EDTA, 10 mM EGTA, 0.5% Brij-35, 10% glycerol, and 2 mM DTT, pH 7.6, supplemented with complete protease inhibitor tablets [Roche]), and the cells were lysed by bead beating at 4°C. Lysates were cleared by centrifugation, and the supernatant were snap frozen in aliquots in liquid nitrogen. 2-ml aliquots were thawed, spun briefly, and the supernatant was injected at a flow rate of 0.1 ml/min onto the affinity column equilibrated and run in 50 mM Na-Hepes, 20 mM NaCl, and 1 mM DTT, pH 7.6, using an FPLC (GE Healthcare). After 30 min, the flow rate was increased to 1 ml/min, the column was washed to ~0.08 OD_{280}, and bound protein was eluted with 50 mM Na-Hepes, 1 M NaCl, and 1 mM DTT, pH 7.6, taking 250-μl fractions. The peak fractions were pooled and snap frozen. Similar protein elution amounts were loaded and separated on 4–12% gradient gels.

Size-exclusion chromatography of Stu2p and free tubulin complexes

Full-length Stu2p, TOG1, or TOG1–TOG2 protein was loaded at 20 μM onto a 10/5 Superose 6 gel filtration column preequilibrated with gel filtration buffer at 4°C (25 mM Tris, 200 mM NaCl, 1 mM $MgCl_2$, and 1 mM EGTA, pH 7.5) and eluted in 0.4-ml fractions. For tubulin-binding experiments, Stu2p or TOG constructs were first dialyzed against running buffer and were then mixed with an equal amount of recycled bovine brain tubulin dimer. Stu2p–tubulin (or TOG–tubulin) complexes were allowed to form for 30 min at 4°C before loading onto a Superose 6 10/300 GL gel filtration column (GE Healthcare). Fractions were evaluated by SDS-PAGE. The protein content of each band was determined from scans of the gels using Image J 1.32j software (National Institutes of Health). Apparent molecular masses and Stokes radii of the Stu2p constructs and tubulin complexes were determined by calibrating the size-exclusion column with the following set of protein standards: thyroglobulin, ferritin, catalase, aldolase, albumin, ovalbumin, chymotrypsinogen, and ribonuclease A. Stokes radii were calculated as averages of the Porath and Laurent-Killander Stokes' radii, which matched closely.

Sedimentation equilibrium analytical ultracentrifugation of the Stu2 and tubulin complex

Sedimentation equilibrium experiments of wild-type Stu2p, TOG1–TOG2, and Stu2-ΔC with and without tubulin were conducted at 4°C in an analytical ultracentrifuge (Optima XLA; Beckman Coulter). Samples corresponding to an absorbance at 280 nm of 0.25–0.75 were prepared in 50 mM Hepes, pH 7.5, 180 mM KCl, 1 mM MgCl2, and 1 mM Tris-(2-carboxyethyl) phosphine. Data were acquired as an average of two absorbance measurements at a nominal wavelength of 280 nm and a radial spacing of 0.001 cm at the rotor speeds indicated for each experiment. In each speed, equilibrium was achieved within 40-h global analyses in terms of a single ideal solute by multiple fit alignment in the XL-I software package (Beckman Coulter) using data from three speeds and protein concentrations to obtain the buoyant molecular mass M(1-νρ).

Electron microscopy of Stu2p and tubulin complexes

Early fractions of each of the gel filtration experiments were evaluated using negative stain electron microscopy. Fractions were diluted to 0.1 mg/ml and incubated on glow discharged continuous carbon support film on 400 copper mesh grids for 5 min. Samples were washed with gel filtration buffer, stained with 0.5% uranyl formate, and dried. Samples were imaged at 52,000× using a microscope (Techni-12; Phillips) operated at 120 kV with a low dose kit. Images were collected on a CCD camera (model 894; Gatan) using Digital Micrograph software (Gatan). Contour lengths of images of free Stu2p dimer along which particle paths could be traced clearly (Fig. S4) were measured using the measuring tool of Image J 1.32 software.

Online supplemental material

Fig. S1 shows a schematic of all constructs used in this study. Fig. S2 shows the size-exclusion chromatography and electron microscopy of the Stu2-ΔC–tubulin complex, quantitative densitometry of Stu2p to tubulin in complexes, titration of TOG1 binding to tubulin, and shows that Stu2-ΔTOG1 does not bind tubulin. Fig. S3 shows analytical ultracentrifugation data of Stu2p and tubulin complexes as well as their curve fits. Fig. S4 shows the heterogeneous conformations of Stu2p in electron microscopy images. Fig. S5 shows data spread and statistics for the slow and fast anaphase spindle elongation velocities shown in Fig. 3. Online supplemental material is available at http://www.jcb.org/cgi/content/full/jcb.200511010/DC1.

We thank D. Drechsel for purification of full-length Stu2p and for goat anti-GFP antibody; P. Sorger for the gift of a Stu2p baculovirus vector; Anna Shevchenko (Max Planck Institute of Molecular Cell Biology and Genetics [MPI-CBG]) for mass spectrometry; Eric Schaefer (MPI-CBG) for help with curve fitting; Wolfgang Zachariae (MPI-CBG) for reagents; Bianca Habermann (MPI-CBG) for alignment of the TOG domain sequences of Stu2p and Dis1/XMAP215 family members; and Anastasia Hoykov (Harvard Medical School, Boston, MA) for preparing insect cells and media. We also thank members of the Harrison lab (Harvard Medical School) and Hyman lab (MPI-CBG) for critically reading this manuscript.

J. Al-Bassam is a postdoctoral fellow of the American Cancer Society. S.C. Harrison is an investigator at the Howard Hughes Medical Institute.

Submitted: 3 November 2005
Accepted: 21 February 2006

References

Brittle, A.L., and H. Ohkura. 2005. Mini spindles, the XMAP215 homologue, suppresses pausing of interphase microtubules in *Drosophila*. *EMBO J.* 24:1387–1396.

Carvalho, P., J.S. Tirnauer, and D. Pellman. 2003. Surfing on microtubule ends. *Trends Cell Biol.* 13:229–237.

Cassimeris, L., and J. Morabito. 2004. TOGp, the human homolog of XMAP215/Dis1, is required for centrosome integrity, spindle pole organization, and bipolar spindle assembly. *Mol. Biol. Cell.* 15:1580–1590.

Cassimeris, L., D. Gard, P.T. Tran, and H.P. Erickson. 2001. XMAP215 is a long thin molecule that does not increase microtubule stiffness. *J. Cell Sci.* 114:3025–3033.

Charrasse, S., M. Schroeder, C. Gauthier-Rouviere, F. Ango, L. Cassimeris, D.L. Gard, and C. Larroque. 1998. The TOGp protein is a new human microtubule-associated protein homologous to the *Xenopus* XMAP215. *J. Cell Sci.* 111:1371–1383.

Desai, A., and T.J. Mitchison. 1997. Microtubule polymerization dynamics. *Annu. Rev. Cell Dev. Biol.* 13:83–117.

Desai, A., S. Verma, T.J. Mitchison, and C.E. Walczak. 1999. Kin I kinesins are microtubule-destabilizing enzymes. *Cell*. 96:69–78.

De Wulf, P., A.D. McAinsh, and P.K. Sorger. 2003. Hierarchical assembly of the budding yeast kinetochore from multiple subcomplexes. *Genes Dev.* 17:2902–2921.

Diamantopoulos, G.S., F. Perez, H.V. Goodson, G. Batelier, R. Melki, T.E. Kreis, and J.E. Rickard. 1999. Dynamic localization of CLIP-170 to microtubule plus ends is coupled to microtubule assembly. *J. Cell Biol.* 144:99–112.

Epstein, C.B., and F.R. Cross. 1992. CLB5: a novel B cyclin from budding yeast with a role in S phase. *Genes Dev.* 6:1695–1706.

Garcia, M.A., L. Vardy, N. Koonrugsa, and T. Toda. 2001. Fission yeast ch-TOG/XMAP215 homologue Alp14 connects mitotic spindles with the kinetochore and is a component of the Mad2-dependent spindle checkpoint. *EMBO J.* 20:3389–3401.

Gard, D.L., and M.W. Kirschner. 1987. A microtubule-associated protein from *Xenopus* eggs that specifically promotes assembly at the plus-end. *J. Cell Biol.* 105:2203–2215.

Gard, D.L., B.E. Becker, and S.J. Romney. 2004. MAPping the eukaryotic tree of life: structure, function, and evolution of the MAP215/Dis1 family of microtubule-associated proteins. *Int. Rev. Cytol.* 239:179–272.

Galjart, N., and F. Perez. 2003. A plus-end raft to control microtubule dynamics and function. *Curr. Opin. Cell Biol.* 15:48–53.

Gergely, F., V.M. Draviam, and J.W. Raff. 2003. The ch-TOG/XMAP215 protein is essential for spindle pole organization in human somatic cells. *Genes Dev.* 17:336–341.

Gräf, R., C. Daunderer, and M. Schliwa. 2000. Dictyostelium DdCP224 is a microtubule-associated protein and a permanent centrosomal resident involved in centrosome duplication. *J. Cell Sci.* 113:1747–1758.

Gräf, R., U. Euteneuer, T.H. Ho, and M. Rehberg. 2003. Regulated expression of the centrosomal protein DdCP224 affects microtubule dynamics and reveals mechanisms for the control of supernumerary centrosome number. *Mol. Biol. Cell*. 14:4067–4074.

He, X., D.R. Rines, C.W. Espelin, and P.K. Sorger. 2001. Molecular analysis of kinetochore-microtubule attachment in budding yeast. *Cell*. 106:195– 206.

Holmfeldt, P., S. Stenmark, and M. Gullberg. 2004. Differential functional interplay of TOGp/XMAP215 and the KinI kinesin MCAK during interphase and mitosis. *EMBO J.* 23:627–637.

Howard, J., and A.A. Hyman. 2003. Dynamics and mechanics of the microtubule plus end. *Nature*. 422:753–758.

Hunter, A.W., M. Caplow, D.L. Coy, W.O. Hancock, S. Diez, L. Wordeman, and J. Howard. 2003. The kinesin-related protein MCAK is a microtubule depolymerase that forms an ATP-hydrolyzing complex at microtubule ends. *Mol. Cell*. 11:445–457.

Kahana, J.A., B.J. Schnapp, and P.A. Silver. 1995. Kinetics of spindle pole body separation in budding yeast. *Proc. Natl. Acad. Sci. USA*. 92:9707–9711.

Kinoshita, K., I. Arnal, A. Desai, D.N. Drechsel, and A.A. Hyman. 2001. Reconstitution of physiological microtubule dynamics using purified components. *Science*. 294:1340–1343.

Kinoshita, K., B. Habermann, and A. Hyman. 2002. XMAP215: a key component of the dynamic microtubule cytoskeleton. *Trends Cell Biol.* 12:267–273.

Kosco, K.A., C.G. Pearson, P.S. Maddox, P.J. Wang, I.R. Adams, E.D. Salmon, K. Bloom, and T.C. Huffaker. 2001. Control of microtubule dynamics by Stu2p is essential for spindle orientation and metaphase chromosome alignment in yeast. *Mol. Biol. Cell*. 12:2870–2880.

Lee, W.L., J.R. Oberle, and J.A. Cooper. 2003. The role of the lissencephaly protein Pac1 during nuclear migration in budding yeast. *J. Cell Biol.* 160:355–364.

Liakopoulos, D., J. Kusch, S. Grava, J. Vogel, and Y. Barral. 2003. Asymmetric loading of Kar9 onto spindle poles and microtubules ensures proper spindle alignment. *Cell*. 112:561–574.

Maekawa, H., T. Usui, M. Knop, and E. Schiebel. 2003. Yeast Cdk1 translocates to the plus end of cytoplasmic microtubules to regulate bud cortex interactions. *EMBO J.* 22:438–449.

Moores, C.A., M. Yu, J. Guo, C. Beraud, R. Sakowicz, and R.A. Milligan. 2002. A mechanism for microtubule depolymerization by KinI kinesins. *Mol. Cell*. 9:903–909.

Nakaseko, Y., K. Nabeshima, K. Kinoshita, and M. Yanagida. 1996. Dissection of fission yeast microtubule associating protein p93Dis1: regions implicated in regulated localization and microtubule interaction. *Genes Cells*. 1:633–644.

Nakaseko, Y., G. Goshima, J. Morishita, and M. Yanagida. 2001. M phase-specific kinetochore proteins in fission yeast: microtubule-associating Dis1 and Mtc1 display rapid separation and segregation during anaphase. *Curr. Biol.* 11:537–549.

Niederstrasser, H., Salehi-Had, H., Gan, E.C., Walczak, C., and E. Nogales. 2002. XKCM1 acts on a single protofilament and requires the C terminus of tubulin. *J. Mol. Biol.* 316: 817–828.

Neef, R., C. Preisinger, J. Sutcliffe, R. Kopajtich, E.A. Nigg, T.U. Mayer, and F.A. Barr. 2003. Phosphorylation of mitotic kinesin-like protein 2 by polo-like kinase 1 is required for cytokinesis. *J. Cell Biol.* 162:863–875.

Ohkura, H., M.A. Garcia, and T. Toda. 2001. Dis1/TOG universal microtubule adaptors – one MAP for all? *J. Cell Sci.* 114:3805–3812.

Perez, F., G.S. Diamantopoulos, R. Stalder, and T.E. Kreis. 1999. CLIP-170 highlights growing microtubule ends in vivo. *Cell*. 96:517–527.

Severin, F., B. Habermann, T. Huffaker, and T. Hyman. 2001. Stu2p promotes mitotic spindle elongation in anaphase. *J. Cell Biol.* 153:435–442.

Sheeman, B., P. Carvalho, I. Sagot, J. Geiser, D. Kho, M.A. Hoyt, and D. Pellman. 2003. Determinants of *S. cerevisiae* dynein localization and activation: implications for the mechanism of spindle positioning. *Curr. Biol.* 13:364–372.

Shirasu-Hiza, M., P. Coughlin, and T. Mitchison. 2003. Identification of XMAP215 as a microtubule-destabilizing factor in *Xenopus* egg extract by biochemical purification. *J. Cell Biol.* 161:349–358.

Spittle, C., S. Charrasse, C. Larroque, and L. Cassimeris. 2000. The ineraction of TOGp with microtubules and tubulin. *J. Biol. Chem.* 275:20748–20753.

Straight, A.F., W.F. Marshall, J.W. Sedat, and A.W. Murray. 1997. Mitosis in living budding yeast: anaphase A but no metaphase plate. *Science*. 277:574–578.

Straight, A.F., J.W. Sedat, and A.W. Murray. 1998. Time-lapse microscopy reveals unique roles for kinesins during anaphase in budding yeast. *J. Cell Biol.* 143:687–694.

Tanaka, K., N. Mukae, H. Dewar, M. van Breugel, E.K. James, A.R. Prescott, C. Antony, and T.U. Tanaka. 2005. Molecular mechanisms for kinetochore capture by spindle microtubules. *Nature*. 434:987–994.

Tournebize, R., A. Popov, K. Kinoshita, A.J. Ashford, S. Rybina, A. Pozniakovsky, T.U. Mayer, C.E. Walczak, E. Karsenti, and A.A. Hyman. 2000. Control of microtubule dynamics by the antagonistic activities of XMAP215 and XKCM1 in *Xenopus* egg extracts. *Nat. Cell Biol.* 2:13–19.

Usui, T., H. Maekawa, G. Pereira, and E. Schiebel. 2003. The XMAP215 homologue Stu2 at yeast spindle pole bodies regulates microtubule dynamics and anchorage. *EMBO J.* 22:4779–4793.

van Breugel, M., D. Drechsel, and A. Hyman. 2003. Stu2p, the budding yeast member of the conserved Dis1/XMAP215 family of microtubule-associated proteins is a plus end-binding microtubule destabilizer. *J. Cell Biol.* 161:359–369.

Vasquez, R.J., D.L. Gard, and L. Cassimeris. 1994. XMAP from *Xenopus* eggs promotes rapid plus end assembly of microtubules and rapid microtubule turnover. *J. Cell Biol.* 127:985–993.

Wang, P.J., and T.C. Huffaker. 1997. Stu2p: A microtubule-binding protein that is an essential component of the yeast spindle pole body. *J. Cell Biol.* 139:1271–1280.

Whittington, A.T., O. Vugrek, K.J. Wei, N.G. Hasenbein, K. Sugimoto, M.C. Rashbrooke, and G.O. Wasteneys. 2001. MOR1 is essential for organising cortical microtubules in plants. *Nature*. 411:610–613.

Yeh, E., R.V. Skibbens, J.W. Cheng, E.D. Salmon, and K. Bloom. 1995. Spindle dynamics and cell cycle regulation of dynein in the budding yeast, *Saccharomyces cerevisiae*. *J. Cell Biol.* 130:687–700.